

## Iron spin waves in $\text{YFe}_2$ and $\text{UFe}_2$

L. Paolasini\*

*Laboratoire Léon Brillouin, Centre National de la Recherche Scientifique—Commissariat à l'Énergie Atomique, CE-Saclay,  
91191 Gif-sur-Yvette, France*

R. Caciuffo

*Istituto Nazionale per la Fisica della Materia, Dipartimento di Scienze dei Materiali della Terra, Università di Ancona,  
Via Breccie Bianche, I-60131 Ancona, Italy*

B. Roessli†

*Institut Laue Langevin, 156X, 38042 Grenoble, France*

G. H. Lander

*European Commission, JRC, Institute for Transuranium Elements, D-76125 Karlsruhe, Germany*

K. Myers and P. Canfield

*Ames Laboratory—Iowa State University, Ames, Iowa 50011*

(Received 24 August 1998)

We report the results of neutron inelastic scattering measurements on single crystals of  $\text{YFe}_2$  and  $\text{UFe}_2$  with special emphasis on the energy region above  $\sim 7$  meV, which was not reported in our earlier work on  $\text{UFe}_2$ . Iron spin waves have been observed up to 55 meV in  $\text{YFe}_2$ , but in  $\text{UFe}_2$  such modes become broad at energies above  $\sim 35$  meV. The most surprising aspects in  $\text{UFe}_2$  are the absence of any observable mode involving the U  $5f$  electrons, and the strong Fe-Fe interactions as judged by the dispersion of the Fe only mode. Since the spectrum in  $\text{YFe}_2$  can be considered as representing “diluted” Fe in the cubic Laves phase structure, it is particularly useful to compare the results for  $\text{UFe}_2$  and  $\text{YFe}_2$ . In addition to the increased Fe-Fe interaction (resulting in a larger spin-wave stiffness than found in pure Fe), there is evidence that the Fe spin wave in  $\text{UFe}_2$  interacts with a  $\Lambda_1$  optic phonon mode in the  $\langle 111 \rangle$  direction. This phonon represents a breathing between the U and Fe sublattices, and we suggest that it is mediated by the hybridization between the U  $5f$  and Fe  $3d$  electrons. [S0163-1829(99)00510-X]

### I. INTRODUCTION

Following extensive investigation of the heavy rare-earth (RE) $\text{Fe}_2$  compounds (fcc Laves phase crystal structure) some 15–20 years ago,<sup>1</sup> there has been a renewal of interest in the isostructural ferromagnets with cerium and uranium stimulated by theoretical advances<sup>2,3</sup> predicting how the spin and orbital moments will change as the itinerant  $f$  electrons hybridize with the  $3d$  electrons of Fe. Neutron form factor, x-ray magnetic circular dichroism, and magnetic x-ray Compton scattering experiments have demonstrated the importance of these hybridization effects in the *static* ground-state properties of both  $\text{CeFe}_2$  (Ref. 4) and  $\text{UFe}_2$ .<sup>5</sup> Our interest in this work is to investigate the effects of hybridization on the *dynamical* response function of these two unusual materials. This subject has not yet been addressed by theory, but we hope that our measurements will provide motivation for such efforts.

In our first publication using inelastic neutron scattering we showed that a number of unusual effects are present in the spin wave response of  $\text{UFe}_2$ .<sup>6</sup> The two most important are that *no* response is seen from the uranium spins, and that the Fe spin-wave response is substantially “hardened” at low temperature when compared to that of pure iron (i.e., at

low temperature the spin-wave stiffness parameter is actually greater than that of pure iron, although  $T_c$  is considerably lower in  $\text{UFe}_2$ ). We have recently completed similar neutron inelastic measurements on single crystals of  $\text{CeFe}_2$ .<sup>7</sup> Of the two points mentioned above, the first is common to the results from  $\text{CeFe}_2$ , i.e., no response is seen from the Ce spins, but, in contrast to the situation in  $\text{UFe}_2$ , the spin-wave stiffness of  $\text{CeFe}_2$  is greatly reduced compared to that found in pure Fe.

Our inability to observe experimentally a response associated directly with the  $f$  element moment in these systems may arise from one (or both) of the following reasons. (1) The response is too weak because the spin moments on both the uranium and cerium ions are of an order of magnitude of  $0.2\mu_B$ , and/or (2) the response from the  $f$  spins is spread over a large energy range. In this latter case, the signal is difficult to separate from the background as the neutron instruments used in these studies, triple-axis spectrometers, have a relatively small resolution ellipsoid in reciprocal space.

The major difference between the compounds  $\text{CeFe}_2$  and  $\text{UFe}_2$  as far as the response of the Fe spins is concerned is certainly surprising, and can be answered only when theoretical estimates of  $\chi''(\mathbf{Q}, \omega)$  are available with which to com

TABLE I. Information on the three Laves phases ferromagnets (all with the C15 fcc crystal structure, symmetry  $Fd\bar{3}m$ ) studied by inelastic neutron scattering. In this structure each Fe has six nearest Fe neighbors. Pure Fe, which is bcc with eight nearest Fe neighbors, is added for comparison.  $T_c$  is the Curie temperature,  $\mu_{\text{Fe}}$  is the magnetic moment on the Fe site, and  $\Delta E$  is the ferromagnetic spin-wave gap at the zone center,  $q=0$ . The spin-wave stiffness constant  $D$  (see text) is shown for 100 K. The final row gives the deduced exchange between the Fe moments—see text. Standard deviations in parentheses refer to the least-significant digit.

	Fe	YFe <sub>2</sub>	CeFe <sub>2</sub>	UFe <sub>2</sub>
$a_0$ (Å) (RT)	2.8665	7.370	7.304	7.057
$d$ (Fe-Fe) Å	2.48	2.61	2.58	2.50
$T_c$ (K)	1043(2)	545(5)	235(5)	165(5)
$\mu_{\text{Fe}}$ ( $\mu_B$ )	2.20(4)	1.5(1)	1.2(1)	0.6(1)
$\Delta E$ (meV)	<0.1	0.21(5)	0.25(3)	0.40(5)
$D$ (meV Å <sup>2</sup> )				
$T=100$ K	325(10)	250(12)	155(5)	440(30)
$J$ (meV)	24.0	24.4	19.4	117
( $\sim \pm 15\%$ )				

pare experiments. Furthermore, measurements of the phonons (at room temperature) for CeFe<sub>2</sub>, YFe<sub>2</sub>, and UFe<sub>2</sub> have shown<sup>8</sup> that the parameters describing the phonons of the former two materials are roughly comparable, whereas in UFe<sub>2</sub> this is not the case. Instead, the phonon parameters in UFe<sub>2</sub> show strong deviations from those expected in a normal Laves-phase material, suggesting that the phonon spectrum is strongly influenced by the electronic susceptibility. Thus, one motivation for the present measurements was to establish whether any direct evidence could be obtained for a magnon-phonon interaction.

Because the Fe moment is only  $0.6\mu_B$  in UFe<sub>2</sub> and thus small, the neutron inelastic experiments are difficult, despite the large ( $\sim 7$  g) single crystal available. Our earlier work extended only to  $\sim 7$  meV energy transfer. Recently, we have reported briefly<sup>9</sup> on measurements up to  $\sim 20$  meV. In this paper we summarize all our work extending the spin-wave measurements up to  $\sim 35$  meV, and we contrast the behavior of the Fe spin waves in the uranium compound with those in YFe<sub>2</sub>. Comparative data, which will be useful in discussing the various compounds, are collected in Table I.

YFe<sub>2</sub> is particularly important in these comparisons. Because trivalent Y has no open  $d$  or  $f$  shell, it may be considered as “diluted” Fe, with the same Laves phase crystal structure as the other interesting materials discussed in this paper.

## II. EXPERIMENTAL DETAILS AND RESULTS

The UFe<sub>2</sub> crystal is the same one described in Ref. 6. Single crystals of YFe<sub>2</sub> were grown in Ames from a Y-rich binary melt. High-purity elements were placed in a sealed Ta crucible and slowly cooled from 1200 °C to 950 °C over a period of a week. After this the excess liquid was decanted from large faceted crystals.

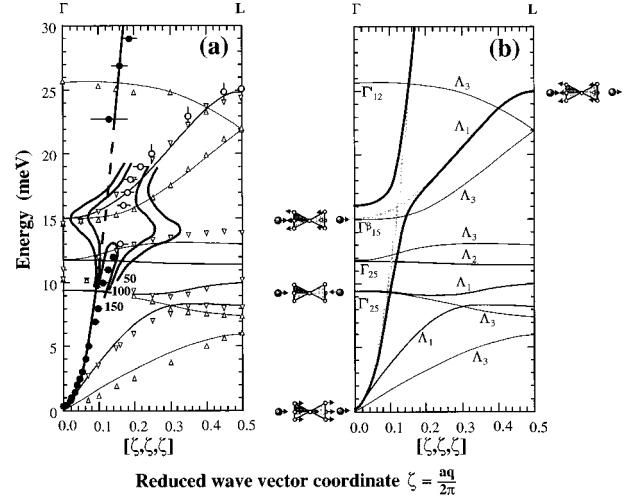


FIG. 1. (a) Spin-wave spectrum at 100 K (filled circles) and phonon dispersion relationships (phonons:  $\Delta$ , transverse;  $\nabla$ , longitudinal) at 300 K in the  $\langle 111 \rangle$  direction. For the spin wave the quadratic relation is shown as a solid line, and clearly holds up to  $\sim 10$  meV. The strong interaction of the spin wave with another mode is shown above  $\sim 13$  meV by contours of equal intensity. The lines through the experimental phonon points represent a fit with a Born–von Kármán model and is discussed in more detail in Ref. 8. The open circles represent what we believe to be a mixed magnon-phonon mode. (b) Simulation of the magnon-phonon interaction proposed in UFe<sub>2</sub>. The lines are guides to the eye. The symmetry of certain phonon modes and their relative displacements at the zone center and boundary are represented by showing  $[111]$  projections of the Fe tetrahedra along with two of the nearest neighbor U ions. For more details on the displacements see Ref. 8.

The neutron inelastic scattering experiments have been performed on the IN8 (thermal) and IN1 (hot) triple-axis spectrometers at the Institut Laue Langevin, Grenoble, and also with the 1T1 (thermal) instrument at the Laboratoire Leon Brillouin, Saclay. In all cases focusing graphite or copper monochromators have been used with graphite filters to suppress higher-order contamination. At the IN8 and IN1 spectrometers at the ILL a horizontal magnet with a field of 0.4 T aligned along the  $\langle 111 \rangle$  axis in the scattering plane assured that a single ferromagnetic domain existed during the experiments. Such an arrangement increases the observed spin-wave intensity by a factor of 50% over that in a multi-domain sample.

To provide an overview before showing individual scans we show in Fig. 1 the most interesting region of the UFe<sub>2</sub> spectra in the  $\langle 111 \rangle$  direction. It should be emphasized, as we did earlier,<sup>6</sup> that *all* this response is associated with the Fe spins. An important question is what happens in the energy range above  $\sim 12$  meV, and it is on this region that we focus in this paper. The dashed line shows the spin-wave response extrapolated from that determined earlier,<sup>6</sup> and it clearly continues to  $\sim 10$  meV before becoming difficult to follow. Some of the scans used to construct Fig. 1 are shown in Fig. 2. The  $\chi''(\mathbf{q}, \omega)$  function is shown on the right-hand side and the shading illustrates how the shape of the peak changes over this energy range. Scans with the IN1 triple-axis spectrometer, which is placed on the hot source at the ILL, and thus able to measure excitations at much higher energy trans-

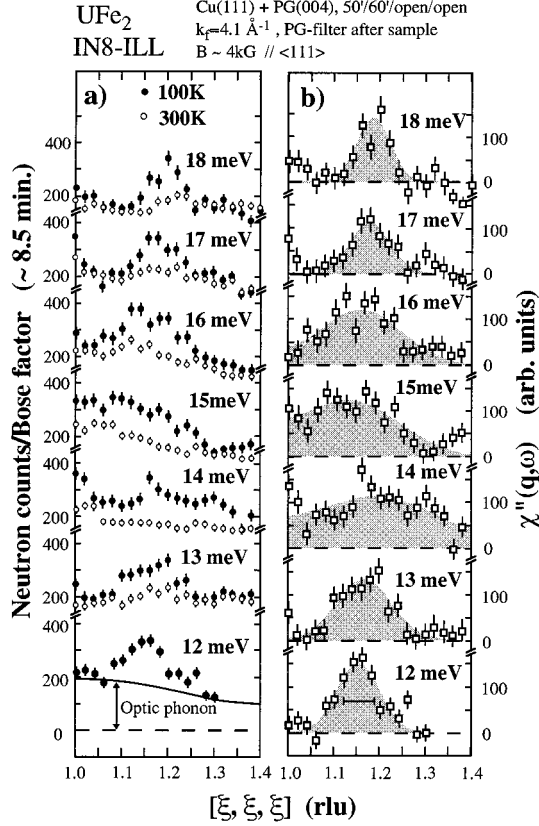


FIG. 2. Data used in the construction of Fig. 1. Data are shown on the left-hand side (a) for both 100 and 300 K. The magnetic signal is much smaller at 300 K, and most of the background is from optic phonons. By performing constant energy scans these phonons do not appear as peaks, as they have little dispersion, see Fig. 1, over this energy range. On the right-hand side (b) is shown the function  $\chi''(\mathbf{q}, \omega)$ , which is obtained by subtracting a background and correcting by the Bose factor. The shading is a guide to the eye. [Data taken with a 0.4 T field along the scattering vector, and using  $k_f=4.1 \text{ \AA}^{-1}$  and  $\text{Cu}(111) \rightarrow \text{PG}(004)$  with IN8 at ILL.]

fer, showed no additional *magnetic* excitations in  $\text{UFe}_2$  above 40 meV. However, some evidence of magnetic scattering is found up to at least 35 meV, even though the excitations are broad. In principle, of course, there will be many additional optic magnetic modes, but they are presumably too weak to be observed with the size of the present crystal and neutron fluxes.

Comparisons between  $\text{YFe}_2$  and  $\text{UFe}_2$  are shown in Fig. 3. The Curie temperature  $T_C$  of  $\text{UFe}_2$  is about a third of that of  $\text{YFe}_2$  (Table I), so that these diagrams represent the situation at low temperature in both compounds, and comparisons are valid despite the different temperatures. The top panel demonstrates the greater stiffness of the  $\text{UFe}_2$  compared to that of  $\text{YFe}_2$ , since in the constant- $E$  mode (see Fig. 1), the excitation comes at a smaller distance from the zone center in  $\text{UFe}_2$ . Considering higher energy the center panel shows the situation along the  $\langle 001 \rangle$  direction. In both materials a propagating spin wave exists, but there is considerably more broadening in the case of  $\text{UFe}_2$ . At 35 meV the dispersion for  $\text{UFe}_2$  is still greater than that for  $\text{YFe}_2$  because the observed peak is closer to the (222) reciprocal lattice point. The

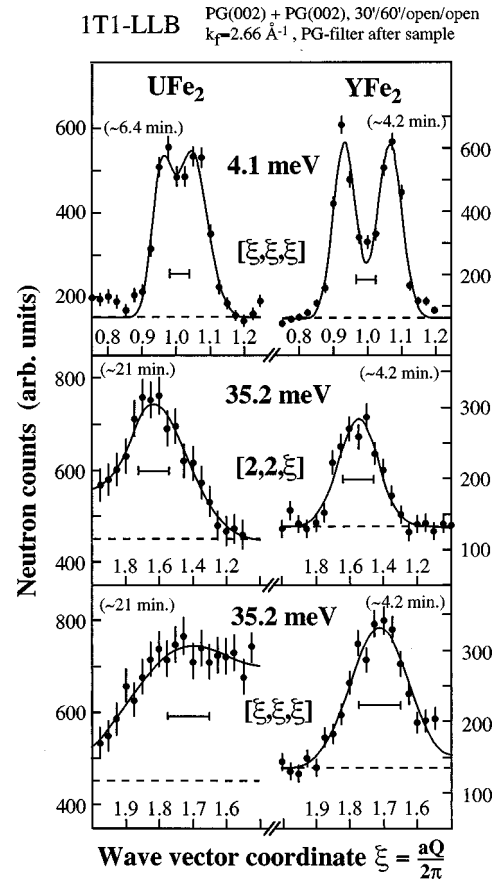


FIG. 3. Scans from  $\text{UFe}_2$  ( $T=50 \text{ K}$ , left-hand side) and  $\text{YFe}_2$  ( $T=300 \text{ K}$ , right-hand side) for different energy transfers. The upper and lower panels are in the  $\langle 111 \rangle$  direction, whereas the center panel is for the momentum transfer in the  $\langle 001 \rangle$  direction. The  $\Gamma$  point for the upper panels is  $\xi=1.0$ ; whereas for the four lower panels it is  $\xi=2.0$ , corresponding to data taken around the reciprocal lattice point [222]. The horizontal bars represent the resolution function of the instrument. (Data from IT1 at LLB.)

lower panel shows the situation at high energy in the  $\langle 111 \rangle$  direction. Here there is clearly only a “ridge” of scattering in the case of  $\text{UFe}_2$ , whereas a well defined excitation still exists for  $\text{YFe}_2$ .

### III. DISCUSSION

Figure 4(a) gives the spin-wave dispersion curve and the calculated phonon spectra<sup>6</sup> for  $\text{YFe}_2$ . The thick solid lines give the fit to the spin-wave dispersion with the relationship

$$E = \Delta E + D(1 - \beta q^2)q^2,$$

where we include only the first higher-order term and assume that  $\beta \sim 1$  following the work on pure iron.<sup>10,11</sup>  $\Delta E$  is the energy gap and  $D$  is the spin-wave stiffness. It is to be noted that the gap is similar to that found in pure Fe; see Table I.  $D$  in pure Fe is  $325 \text{ meV \AA}^2$ . We can use the relationship given in Ref. 10 to deduce the exchange interaction,  $J$ , between the Fe moments. In the approximation of small wave vector  $q$ , the spin-wave stiffness  $D$  is given by  $D = 2JSa^2$ , where  $S$  is the effective spin and  $a$  is the distance between atoms.

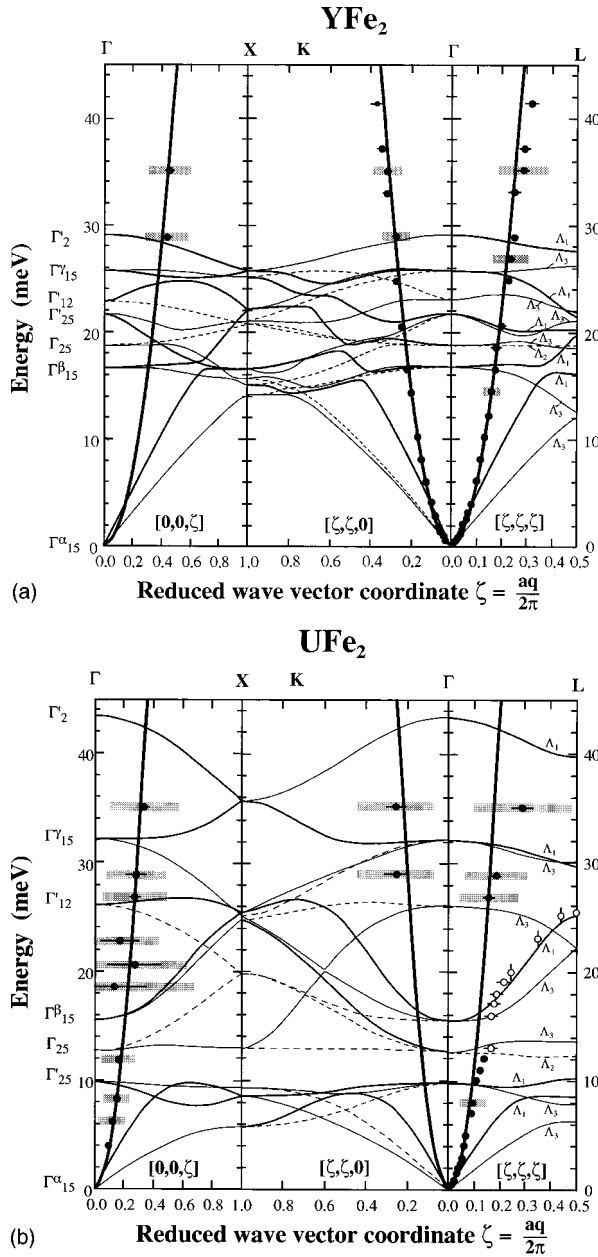


FIG. 4. (a) Spin-wave dispersion curve and calculated phonon spectra (Ref. 8) for  $\text{YFe}_2$  at 300 K. The filled points represent the measured spin-wave energies and the thick solid line is a fit. Shading is an attempt to represent the width of the measured spin wave, and has been shown only for a series of scans taken with similar instrumental parameters. Below 14 meV the spin waves are resolution limited. Fitting to the spin-wave relationship gives  $D = 250$  (12)  $\text{meV} \text{ \AA}^2$ . Thin solid lines represent calculated phonon spectra, with dashed lines showing phonons forbidden in the geometry of the experiment. (b) Spin-wave dispersion curve and calculated phonon spectra for  $\text{UFe}_2$  at 100 K. Symbols are the same as in (a). The open points represent the ‘‘mixed’’ magnon and the  $\Lambda_1$  phonon. The fitting to the low-energy part of the spin wave is with  $D = 440$  (25)  $\text{meV} \text{ \AA}^2$ . Note the much greater broadening of the spin waves in  $\text{UFe}_2$  than in  $\text{YFe}_2$ .

Having deduced  $D$  from the experimental dispersion curves, the other parameters in Table I then allow a deduction of the exchange interaction  $J$ , and this is given in the final row of Table I. Clearly the exchange interaction between Fe mo-

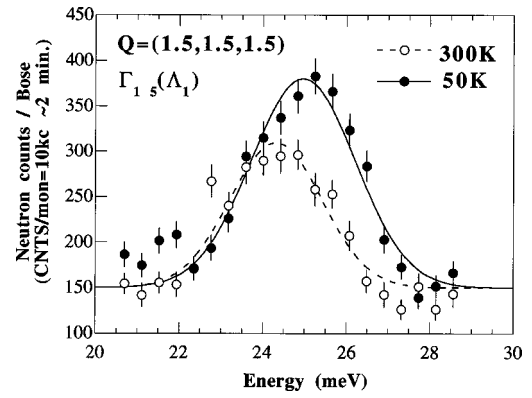


FIG. 5. Data taken at the zone boundary  $L$  point,  $\mathbf{Q} = (1.5, 1.5, 1.5)$  at 50 (closed) and 300 K (open points). To compare the data, the signals have been divided by the respective Bose factors at each energy and temperature. (Data taken at 1T1 at LLB.)

ments in pure Fe and  $\text{YFe}_2$  is exactly the same, and the reduction in  $D$  simply comes from the smaller moment and the larger spacing between Fe atoms. This is further confirmation of our statement that  $\text{YFe}_2$  is simply ‘‘diluted’’ Fe in the Laves-phase crystal structure. On the other hand, there is a fall in  $J$  for  $\text{CeFe}_2$ , consistent with hybridization effects found in that material and the tendency for antiferromagnetic fluctuations.<sup>7</sup> The  $J$  value for  $\text{UFe}_2$  is large—as pointed out previously.<sup>6</sup>

Figure 4(b) shows the spin-wave relationship and the calculated phonon spectra in  $\text{UFe}_2$ . The Fe spin wave in  $\text{UFe}_2$  has a much greater width, especially at higher energy, than those found in  $\text{YFe}_2$ , but magnetic scattering can be observed up to  $\sim 35$  meV.

Focusing now on the interaction with the  $\Lambda_1$  optic mode we show experimental data taken at two temperatures at the zone boundary in Fig. 5. Two unusual aspects may be observed once we have normalized the data by the Bose factors for the different temperatures. The first is that there is *more* intensity at 50 K. We have found, as expected, that all other phonons examined, whether in  $\text{UFe}_2$  or in  $\text{YFe}_2$  obey well the Bose population factors. The second is that the frequency is significantly shifted at 50 K and is higher. Although a small hardening of the phonon spectra might be expected at lower temperature, this shift of  $\sim 5\%$ , although small, is not observed in the lower energy phonons in  $\text{UFe}_2$  on cooling from 300 to 50 K, and this despite a greater precision in the measurement of the lower-energy phonon frequencies.

The  $\Lambda_1$  optic phonon—at least at the zone center—may be visualized as a breathing mode in which the Fe tetrahedra and U ions move alternatively towards and away from each other. This is represented by the small figures on each side of Fig. 1(b), which gives a schematic idea of how the interaction may occur between the spin wave and the  $\Lambda_1$  phonon in the  $\langle 111 \rangle$  direction. Table II shows the vibrational amplitudes of the longitudinal  $\Gamma_{15}^{\beta}(\Lambda_1)$  phonon branch propagating in the  $\langle 111 \rangle$  direction evaluated for different reduced wave vectors  $\mathbf{k} = (\zeta, \zeta, \zeta)$  ( $\zeta = 0.0, 0.1, \dots, 0.5$ ) and expressed in term of absolute values of the Cartesian components. The atom displacements can be expressed in term of eigenvectors  $\{e(\kappa|\mathbf{k})\}$  corresponding to the eigenvalues  $\{\omega^2(\mathbf{k})\}$  of the dynamical matrix  $D(\mathbf{k})$ .<sup>12</sup> The displacement pattern can be described by the Cartesian component  $u_{\alpha}(l\kappa)$  ( $\alpha = x, y, z$ ) of

TABLE II. Vibrational amplitudes  $u_\alpha(l\kappa)$  of the longitudinal  $\Gamma_{15}^\beta(\Lambda_1)$  phonon branch, calculated at different propagation vectors  $\mathbf{k}$ , with coordinates  $(\zeta\zeta\zeta)$  along the  $[111]$  direction. The atoms positions  $U(\kappa)$  and  $\text{Fe}(\kappa)$  label the cluster shown in Fig. 6. The displacements of the Fe atoms 5, 6, and 7, are the same as those of atoms 2, 3, 4, respectively.

Atom positions			Vibrational amplitudes $u_\alpha(l\kappa)$ of $\Gamma_{15}^\beta(\Lambda_1)$ phonon (arb. units)					
			$\zeta=0$	$\zeta=0.1$	$\zeta=0.2$	$\zeta=0.3$	$\zeta=0.4$	$\zeta=0.5$
U(1)	x	1/8	-0.143	0.129	0.093	-0.054	-0.035	0.033
	y	1/8	-0.143	0.129	0.093	-0.054	-0.035	0.033
	z	1/8	-0.143	0.129	0.093	-0.054	-0.035	0.033
U(2)	x	7/8	-0.143	0.129	0.093	-0.054	-0.035	0.033
	y	7/8	-0.143	0.129	0.093	-0.054	-0.035	0.033
	z	7/8	-0.143	0.129	0.093	-0.054	-0.035	0.033
Fe(1)	x	1/2	0.465	-0.475	-0.485	0.460	0.353	0.000
	y	1/2	0.465	-0.475	-0.485	0.460	0.353	0.000
	z	1/2	0.465	-0.475	-0.485	0.460	0.353	0.000
Fe(2)	x	1/2	0.144	-0.166	-0.228	0.311	0.420	0.520
	y	-3/4	0.305	-0.317	-0.344	0.363	0.378	0.398
	z	3/4	0.305	-0.317	-0.334	0.363	0.378	0.398
Fe(3)	x	3/4	0.305	-0.317	-0.334	0.363	0.378	0.398
	y	1/2	0.144	-0.166	-0.228	0.311	0.420	0.520
	z	3/4	0.305	-0.317	-0.334	0.363	0.378	0.398
Fe(4)	x	3/4	0.305	-0.317	-0.334	0.363	0.378	0.398
	y	3/4	0.305	-0.317	-0.334	0.363	0.378	0.398
	z	1/2	0.144	-0.166	-0.228	0.311	0.420	0.520

the  $\kappa$  atom inside the  $l$ -unit cell and associated with the normal mode  $j$  with propagation vector  $\mathbf{k}$  and frequency  $\omega(\mathbf{k})$

$$u_\alpha(l\kappa) = [u(\mathbf{k})e_\alpha(\kappa|\mathbf{k})_j/M_\kappa^{1/2}] \exp\{i[\mathbf{k} \cdot \mathbf{x}(l) - \omega_j(\mathbf{k})t]\},$$

where  $u(\mathbf{k})$  is an arbitrary amplitude factor. We consider the cluster shown in Fig. 6 in which two adjacent Fe tetrahedrons are shown along the  $[111]$  direction, identified as  $\text{Fe}(\kappa)$

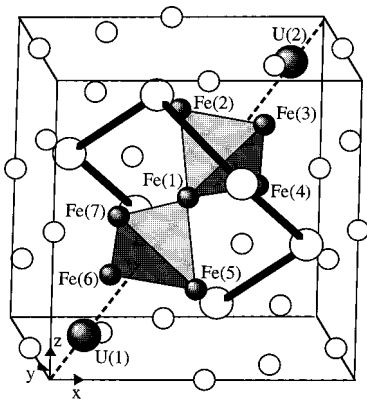


FIG. 6. Crystal structure of cubic Laves phase C15. This is the alternative setting than normally shown, with the U atoms not at the origin, but it places the Fe(1) atom at the body-centered position. Small (large) symbols represent the Fe (U) atoms and those shaded represent the cluster used for the calculation of vibrational amplitudes. The thick lines show the U-U bonding which forms a distorted ring around the central Fe(1) atom.

( $\kappa=1,\dots,7$ ) and two uranium atoms  $U(\kappa)$  ( $\kappa=1,2$ ) also along the  $[111]$ . As shown in Table II, the polarization of Fe(1) is opposite to that of the two U atoms and becomes zero at the zone boundary  $L$ ; see also Fig. 1(b). The other Fe atoms have a quasilongitudinal polarization, but it is not precisely along  $\langle 111 \rangle$ . The Fe atoms on either side of Fe(1) move in phase, and at the zone boundary it is the center Fe atom that is stationary, resulting in a higher energy for this mode. This optic mode results in a strong interaction between the Fe and U wave functions.

The nearest  $d(\text{U-Fe})=2.93 \text{ \AA}$ . If we take the Hill criterion for U-U hybridization as  $3.4 \text{ \AA}$ , then the effective radius is  $1.7 \text{ \AA}$ , and that for Fe (as taken from the nearest neighbor in pure Fe) is  $1.24 \text{ \AA}$ , so that the sum of these radii are  $2.94 \text{ \AA}$ , exactly that for the nearest U-Fe distance in  $\text{UFe}_2$ . According to the phonon spectrum<sup>8</sup> the energy necessary to excite this breathing motion is between 10 and 14 meV at the zone center. This is *exactly* the energy at which it becomes difficult to observe the spin wave in the  $\langle 111 \rangle$  direction, which also represents the closest approach of the two sublattices.

Of course, the ideal measurement would be to perform polarization analysis of the neutron spectra over this energy range, but in view of the weakness of the spin wave scattering in  $\text{UFe}_2$  and the great loss associated with polarization analysis at these energy transfers, this is unfortunately beyond our present capabilities.

As discussed in our earlier work,<sup>6</sup> Eremenko *et al.*<sup>13</sup> introduced the idea of magnon-phonon coupling to explain the large change in the Lamb-Mössbauer factor observed at  $T_C$

in  $\text{UFe}_2$ . They assumed a coupling to the *acoustic* transverse phonons at low energy. There is no evidence for such a coupling, and the anomaly in the Lamb-Mössbauer factor is probably related to the large exchange interactions present in  $\text{UFe}_2$ . However, interestingly, our present measurements do show that there is a possible magnon-phonon interaction, but with the *optic* longitudinal phonons. Schematically, following Ref. 13, we may represent the two modes as shown in Fig. 1(b). Further details of such an interaction, and conse-

quences to the elastic constants, for example, are beyond the scope of the present experimental study.

#### ACKNOWLEDGMENTS

We appreciate discussions with Bernard Hennion. Ames Laboratory is operated for the US DOE by Iowa State University under Contract No. W-7405-Eng-82. This work was supported by the Director for Energy Research, Office of Basic Energy Sciences.

\*Present address: ESRF, B.P. 220 X, F-38043 Grenoble Cedex 9, France.

†Present address: Laboratory for Neutron Scattering, ETH Zürich and PSI, CH-5232 Villigen, Switzerland.

<sup>1</sup>See A. Clark, in *Ferromagnetic Materials*, edited by E. P. Wohlfarth (North-Holland, Amsterdam, 1980), Vol. 1, p. 397; K. Clausen, J. J. Rhyne, B. Lebech, and N. C. Koon, *J. Phys. C* **15**, 3587 (1982); J. J. Rhyne, *J. Magn. Magn. Mater.* **70**, 88 (1987).

<sup>2</sup>M. S. S. Brooks, O. Eriksson, B. Johansson, J. J. M. Franse, and P. H. Frings, *J. Phys. F* **18**, L33 (1988).

<sup>3</sup>O. Eriksson, L. Nördström, M. S. S. Brooks, and B. Johansson, *Phys. Rev. Lett.* **60**, 2523 (1988).

<sup>4</sup>See, for example, M. J. Cooper, P. K. Lawson, M. A. G. Dixon, E. Zukowski, D. N. Timms, F. Itoh, H. Sakurai, H. Kawata, I. Tanaka, and M. Ito, *Phys. Rev. B* **54**, 4068 (1996) and references therein.

<sup>5</sup>G. H. Lander, M. S. S. Brooks, and B. Johansson, *Phys. Rev. B* **43**, 13 672 (1991).

<sup>6</sup>L. Paolasini, G. H. Lander, S. M. Shapiro, R. Caciuffo, B. Le-

ech, L.-P. Regnault, B. Roessli, and J.-M. Fournier, *Europhys. Lett.* **34**, 459 (1996); *Phys. Rev. B* **54**, 7222 (1996).

<sup>7</sup>P. Dervenagas, L. Paolasini, A. Hiess, G. H. Lander, A. Panchula, and P. Canfield, *Physica B* **241-243**, 649 (1998); L. Paolasini, P. Dervenagas, P. Vulliet, J.-P. Sanchez, G. H. Lander, A. Hiess, A. Panchula, and P. Canfield, *Phys. Rev. B* **58**, 12 117 (1998).

<sup>8</sup>L. Paolasini, B. Hennion, A. Panchula, K. Myers, and P. Canfield, *Phys. Rev. B* **58**, 12 125 (1998).

<sup>9</sup>L. Paolasini, R. Caciuffo, B. Roessli, and G. H. Lander, *Physica B* **241-243**, 681 (1998).

<sup>10</sup>G. Shirane, V. J. Minkiewicz, and R. Nathans, *J. Appl. Phys.* **39**, 383 (1968).

<sup>11</sup>M. F. Collins, V. J. Minkiewicz, R. Nathans, L. Passell, and G. Shirane, *Phys. Rev.* **179**, 417 (1969).

<sup>12</sup>A. A. Maradudin and S. H. Vosko, *Rev. Mod. Phys.* **40**, 1 (1968); J. L. Warren, *ibid.* **40**, 38 (1968).

<sup>13</sup>V. V. Eremenko, N. E. Kaner, and V. D. Checherskii, *Sov. Phys. JETP* **67**, 2093 (1988).